The Polarization Lidar Technique for Cloud Research: A Review and Current Assessment

Kenneth Sassen
Department of Meteorology
University of Utah
Salt Lake City, UT

Abstract

The development of the polarization lidar field over the past two decades is reviewed, and the current cloud-research capabilities and limitations are evaluated. Relying on fundamental scattering principles governing the interaction of polarized laser light with distinctly shaped hydrometers, this remote-sensing technique has contributed to our knowledge of the composition and structure of a variety of cloud types. For example, polarization lidar is a key component of current climate-research programs to characterize the properties of cirrus clouds, and is an integral part of multiple remote-sensor studies of mixed-phase cloud systems, such as winter mountain storms. Although unambiguous cloud-phase discrimination and the identification of some ice particle types and orientations are demonstrated capabilities, recent theoretical approaches involving ice crystal ray-tracing and cloud microphysical model simulations are promising to increase the utility of the technique. New results simulating the single and multiple scattering properties of precipitating mixed-phase clouds are given for illustration of such methods.

1. Introduction

It has been two decades since the publication of the first polarization lidar cloud measurements (Schotland et al. 1971), and it seems appropriate to review our progress, assess our current capabilities and limitations, and look toward the future. It is certain that the future of this field is promising, not only because of improving technologies, but more fundamentally because polarization lidar will likely play a key role in making crucial scientific and societal decisions regarding the future of our planet. In view of prospects for climatic change induced by fossil-fuel consumption and various other human activities, it is clear that polarization lidar occupies a special scientific niche of importance to understanding the cloud-climate feedback problem. This is not to minimize the importance of other lidar (see Collis and Russell 1976; Carswell 1983), microwave radar, and passive remote-sensing techniques, for in truth a multiple remote-sensor approach is required for the characterization of the cloudy atmosphere, but polarization lidar is a highly worthwhile, if not indispensable, element of such an instrument ensemble. Major research programs, such as the First International Satellite Cloud Climatology Project Regional Experiment (FIRE), the Experimental Cloud Lidar Pilot Study (ECLIPS), and Atmospheric Radiation Measurement (ARM) projects, are emphasizing the use of polarization lidar for climate-related cloud studies. Indeed, the 1986 Wisconsin FIRE Intensive Field Observation project can be viewed as the first true lidar cloud experiment, in which three of the five participating ground-based and airborne lidars displayed polarization diversity (Sassen et al. 1990a).

The laser backscatter depolarization technique was one of the earliest applications of lidar for atmospheric research. It was borrowed from the analogous microwave radar technique and tested soon after high-powered, short-pulsed lasers became available in the mid-1960s. Unlike radar methods, however, the additional optical receiver components needed for basic depolarization measurements are minimal and involve only a polarization beam-splitter and an extra photodetector. (Radar depolarization observations necessitate the use of an extra dish, although both lidar and radar polarization data have been obtained with one-channel sequential sampling methods.) A basic data quantity is the linear depolarization ratio, or δ value, defined as the ratio of returned powers in the planes of the polarization orthogonal and parallel to that of the linearly polarized source. As shown by Schotland et al. (1971), δ is equivalent to the ratio of the cloud volume backscattering coefficients in the two planes, since all other terms (and unknowns) in the lidar equation (fortunately) drop out when ratioed. It was immediately apparent that lidar δ values in the backscatter from clouds varied over a considerably larger range than those at microwave frequencies. By implication, polarization lidar displayed the potential for remotely sensing the basic microphysical properties of clouds and precipitation, which were only then beginning to come under the scrutiny of more advanced (i.e., laser-based) in situ probes.

In this paper we review the development of the polarization diversity lidar field and the research applications for which it has been shown to be suited (as well as remaining problem areas), and discuss the future of this technique. The discussion is divided into sections, covering the research of the 1970s, when polarization techniques were assessed in the laboratory and by limited lidar field experiments; the 1980s,

when lidar made the full transition to the field (often as part of an integrated instrument ensemble); and the 1990s and beyond, where advanced technologies, and realistic cloud-particle scattering and microphysical simulations will likely provide the basis for enhanced research applications.

2. The basics established

The decade of the 1970s saw the foundations laid for the current cloud research applications of polarization lidar. Various types of hydrometeors were probed in an exploratory fashion, usually from out of a laboratory window, and experimentation with additional polarization techniques was conducted. Research groups reporting polarization-lidar cloud measurements by the mid-1970s included New York University (and subsequently the University of Wyoming using the same equipment), the Hebrew University of Jerusalem, York University of Toronto, the NOAA Wave Propagation Laboratory, and laboratories in Australia and the USSR. (Note that several other groups were by then actively involved in lidar atmospheric research not pertaining to polarization techniques.) Importantly, however, much progress in evaluating atmospheric lidar returns came from laboratory and field experiments using continuous-wave (CW) laser/lidar analog devices. Since optical scattering theory for nonspherical particles was lacking (i.e., lidar investigators could not benefit from the Rayleigh approximation to the Mie theory of our radar investigator colleagues), and only limited lidar studies with ground or air truth support were attempted, the ability to directly compare the δ value to a collected sample of hydrometers was quite useful.

Despite the lack of a working hydrometer scattering theory, though, it was well known that the basic utility of the polarization-lidar technique (i.e., the remote discrimination of water- and ice-phase clouds) was rooted in fundamental scattering theory. Spherically symmetrical and optically homogeneous scatterers, such as cloud and drizzle drops, generate no depolarization of the incident energy in the exact backscattering direction, while scatterers with the arbitrary geometry of ice particles, on the other hand, should generate copious amounts of depolarization. According to Mie theory, droplets backscatter through a combination of axial and paraxial reflections and surface waves, which do not change the incident polarization state, whereas the backscatter from ice crystals, according to ray-tracing theory, normally emerges after internal reflections that rotate the incident polarization plane, leading to depolarization. This basic principle was supported by the initial field and laboratory research reported in Schotland et al. (1971), and soon confirmed by additional laboratory experiments (Liou and Lahore 1974; Sassen 1974). Near-zero δ values for water clouds and $\delta \cong 0.5$ for ice clouds were found by Sassen (1974), and since intermediate values were measured in mixed-phase clouds, it was suggested that a potential existed for remotely determining a measure of cloud ice–water balance.

Subsequent in situ experimentation with natural precipitation elements illustrated that ice particle riming (leading to graupel formation) and snowflake melting effects produced increased depolarization, with maximum $\delta \cong 0.7$ being observed in both cases (Sassen 1975). An analogous microwave radar depolarization "bright band" from melting snowflakes had previously been identified. The source of the increased depolarization over the pristine ice particle was attributed to the increased surface complexity of the particles, either due to the coating of frozen droplets or the presence of the extra water–ice interfaces during melting, which encouraged more complex backscattering ray paths and the further reorientation of the incident laser electric-field vector. Differences in the depolarizing behaviors of individual laboratory-grown ice crystals as a function of crystal habit were also detected (Sassen 1977a). These differences were attributed to the relative importance of nondepolarizing specular reflections (off the large basal or prism faces of pristine crystals) in relation to the internal face areas involved in reflections into the backward direction, which are a function of basic crystal habit (see Fig. 1). In more complex particles such as radiating crystals and aggregates, individual scattering events depended on the orientation of each crystal element relative to the incident beam, and interbranch scatterings were inherent in producing backscattering. Thus, as illustrated in Fig. 2, different types of natural ice particles produced various ranges of single-particle δ values depending on the dominance of fortuitous specular reflections, complex internal ray paths, or interbranch scatterings, but the integrated δ values in most snowfall typically fell within the range of 0.5 ± 0.05, provided the particles were not significantly rimed or melted.

Figure 3 sums up the state of knowledge derived from the laboratory experimental approach. If these CW laser/lidar analog findings could be shown to be applicable to the probing of atmospheric clouds, then it was obvious that detailed cloud microphysical information could be recovered from the lidar δ value. Although the potential for systematic errors in lidar depolarization measurements must be acknowledged, it is important to recognize that, for a given system, even rather small relative differences in δ may reveal important information on changes in hydrometer phase, shape, and condition.

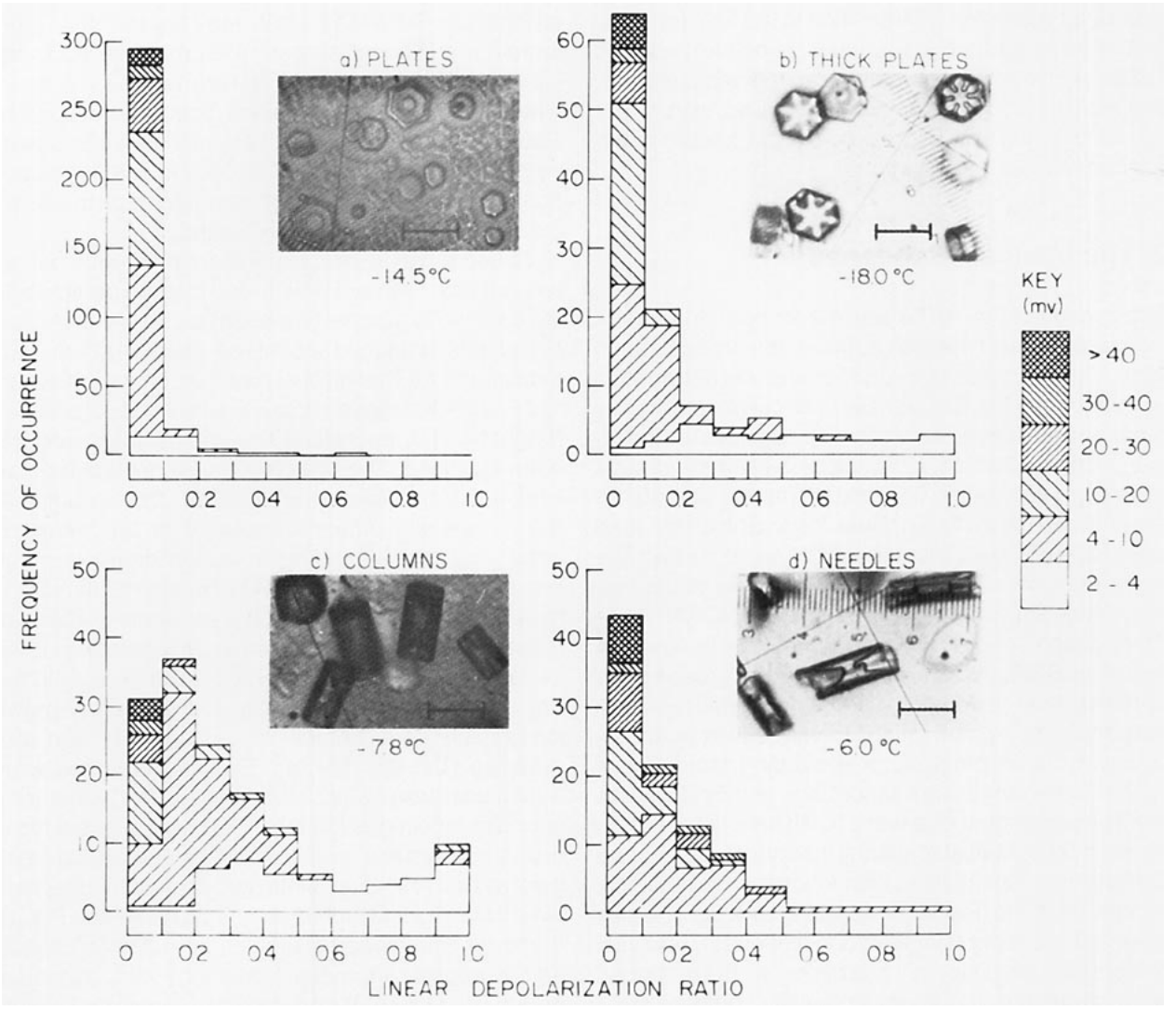

FIG. 1. CW laser backscatter depolarization data obtained in the CSU isothermal cloud chamber, showing differences in δ values as functions of the relative parallel-polarized intensity (see millivolt scale) and basic ice crystal habit (note the 50-μm bars in the inserted photomicrographs). Specular reflections are both intense and nondepolarized, whereas relatively strong depolarized scatterings only occur in prismatic crystals with their large basal-face internal reflecting areas. Only a small fraction of the total (i.e., the most intense) single-particle scattering events were detected (from Sassen 1977a).

Polarization-lidar field research during this decade was exploratory, and often directed toward confirming the encouraging laboratory findings. In general, although some expected (and unexpected) complications to data interpretation were encountered during the field studies, the accumulating body of polarization measurements from atmospheric clouds tended to confirm the basic utility of the technique, as well as lend support to the likelihood of retrieving more detailed ice microphysical data. As in Schotland et al. (1971), it was obvious that liquid clouds and ice particles produced quite different depolarization signatures (Pal and Carswell 1973, 1976, 1977; Cohen 1975; Derr et al. 1976; Sassen 1976b, 1977b,c; Platt 1977). In snowfall and most types of ice clouds, δ values ranged from about 0.2 to 0.8, although most reports were within the 0.4 to 0.5 range, in general agreement with laboratory findings. The lidar depolarization bright band was confirmed in melting snowfall (Sassen 1976b) and thunderstorm precipitation (Sassen 1977b). The first coordinated research aircraft and ground-based polarization-lidar studies in 1976 provided evidence for the predicted depolarization increases due to ice particle riming in orographic clouds (Sassen 1978). And, as had been shown in glaciated laboratory clouds (Sassen 1974), significant δ value increases were measured in supercooled altocumulus clouds following aerial cloud-seeding activities (Sassen 1980).

However, not all atmospheric measurements proved

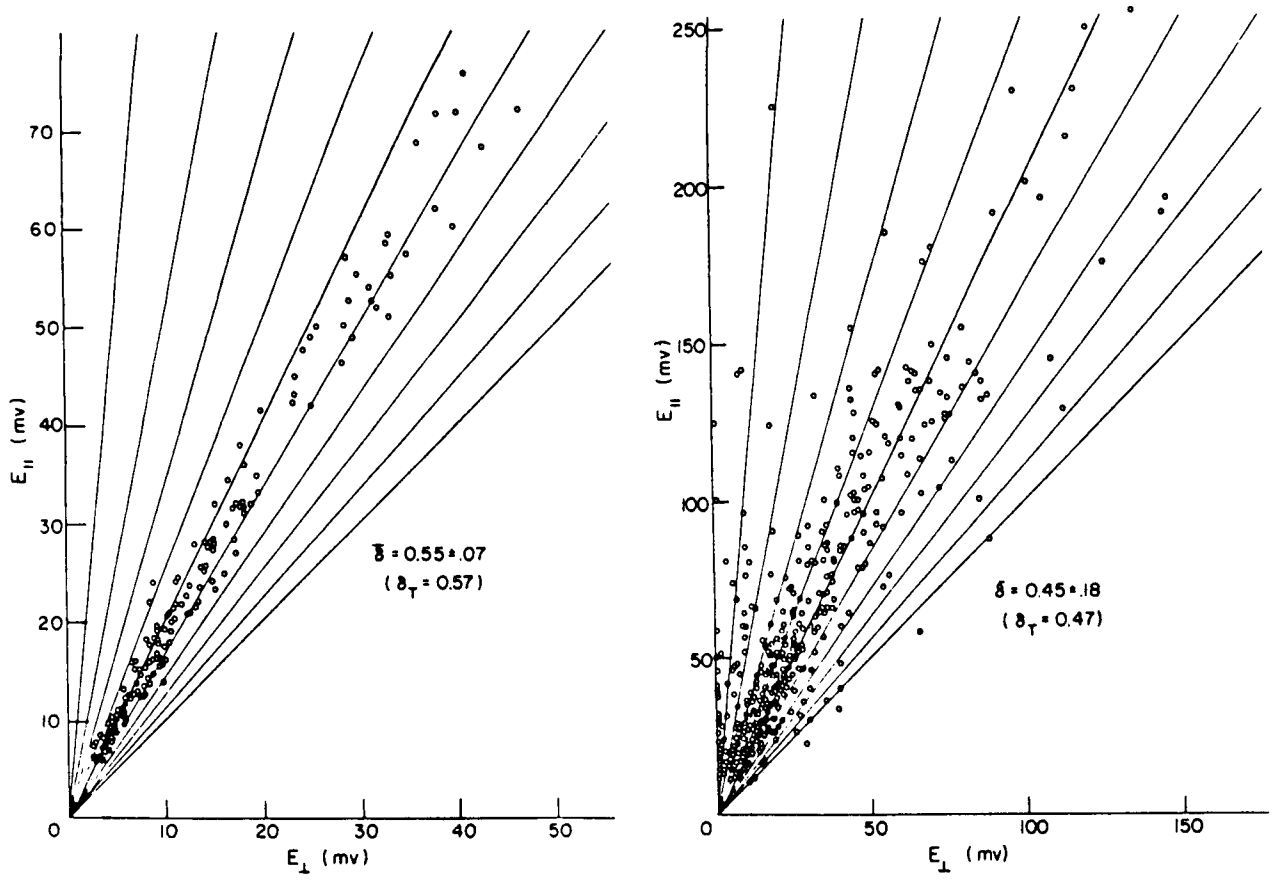

FIG. 2. Plots of a single-particle backscatter energies (in relative units) in the parallel ($E_{\parallel}$) and orthogonal ($E_{\perp}$) polarization planes, from lightly-to-moderately rimed spatial crystals (left), and dendritic ice crystal aggregates (right) sampled by a CW laser/lidar analog device at a mountain-top observatory (from Sassen 1976a). The radiating lines represent 0.1 intervals, and the average and total ($\delta_T = \Sigma E_{\perp}/\Sigma E_{\parallel}$, equivalent to an instantaneous lidar return) depolarization ratios are given. The data at left display relatively small deviations due to the combined effects of frozen cloud droplet and interbranch scattering events, whereas the aggregate ratios vary widely from the impact of a range of simple specular and complex scattering events.

to be so readily comprehensible. First of all, some ice clouds generated $\delta \leq 0.03$, while others defied expectations by producing $\delta \geq 1.0$ (a $\delta = 1.0$ limit for a diffuse scattering medium was expected). The cause of the exceptionally low and high ice-cloud δ values was soon linked to assemblies of uniformly oriented pristine ice crystals, of sizes that could not generally be produced in the laboratory. In the laboratory cloud chamber, the specular reflections from widely fluttering plate crystals were revealed by parallel-polarized signal spikes (Sassen 1974, 1977a), but populations of horizontally oriented plates in the atmosphere produced intensely scattering layers displaying near-zero δ values if the lidar was pointed at or very close to the zenith direction (Platt 1978; Platt et al. 1978). Figure 4 clearly illustrates that this highly anisotropic medium can be identified by scanning the lidar a few degrees off the vertical, a very important operational capability for lidar so as to avoid confusing such returns with liquid water layers (see Platt 1977). (Actually, a tipping angle of ~2.5° is sufficient to identify the majority of these situations, showing that, when oriented, ice plates tend not to flutter much from their stable horizontal orientation.) The occurrences of $\delta \geq 1.0$ were presumed to be a consequence of the same phenomenon when viewed at lower elevation angles, except that a propagation effect induced by laser-pulse transmission through the birefringent ice plates was indicated (Derr et al. 1976; Sassen 1976b). [Ray-tracing simulations by Takano and Jayaweera (1985) later confirmed this deduction.]

Furthermore, the amounts of depolarization generated through photon multiple scattering between droplets in water clouds proved in many cases to be much greater than theoretical simulations had predicted, a finding that, in principle, jeopardized water and ice-cloud phase discrimination. Theoretical simulations (Liou and Schotland 1971; Liou 1972; Eloranta 1972) had shown a characteristic multiple-scattering depolarization signature, in which the δ values gradually

increased (from zero) with height above cloud base, but the strengths of the δ increase did not generally seem to be comparable to field measurements (see Fig. 5). The numerical experiments, however, revealed that the depolarization was controlled by a number of factors, which included lidar beamwidth geometry, cloud droplet concentration and size distribution, and distance to cloud base. It was quite difficult to evaluate the effects of such factors from limited ground-based lidar field campaigns, but special lidar receiver stop designs (Allen and Platt 1977) and four-component (i.e., complete Stokes) polarization measurements (Houston and Carswell 1978) were tested in attempts to achieve the separation of the single- and multiple-scattered components of the lidar return. Controlled laboratory experiments in dense water-droplet clouds were also initiated (Ryan et al. 1979).

To conclude this section, we present in Fig. 6 examples of paired parallel ($P_{||}$) and orthogonal ($P_{\perp}$) polarization-lidar returns from three distinct cloud systems. (These data were collected in 1981 by our mobile lidar system with the aid of an early digital oscilloscope, which was a vast improvement over analog oscilloscope A-scope photography, but before the availability of microcomputer-based data-acquisition systems.) Given are lidar profiles obtained from a drizzle-producing marine stratus layer (on the California coast), showing only multiple scattering depolarization, a spring thunderstorm shower in the Great Basin, and a typical midlatitude cirrus cloud. Illustrated are the depolarization signatures associated with the fundamental microphysical processes of warm-cloud coalescence, *rain from melting snow (i.e., the bright* band), and pure ice-phase precipitation-generating mechanisms.

3. Out of the laboratory

By the early 1980s, a number of field-worthy polarization-lidar systems were being applied to specific cloud-research programs. This transition to the field was typically accomplished (and funded) as part of a multiple remote-sensor approach, initially, perhaps, because of the depth-of-probing limitations of lidar under many cloudy conditions, but later on in recognition of the synergism gained from combined, multiple-wavelength, passive and active remote-sensing observations. Coordinated research aircraft and polarization-lidar investigations became more routine, as was a considerably more international participation in the field. In recognition of the increased cloud microphysical information content, polarization diversity was added to a lidar system that was the first to "winter" the Antarctic (Smiley and Morley 1981). The cloud types that received the most attention were cirrus and winter mountain-storm cloud systems.

Since cirrus clouds are normally rather transparent to lidar probing and contain information on cloud structures and generation mechanisms that are re-

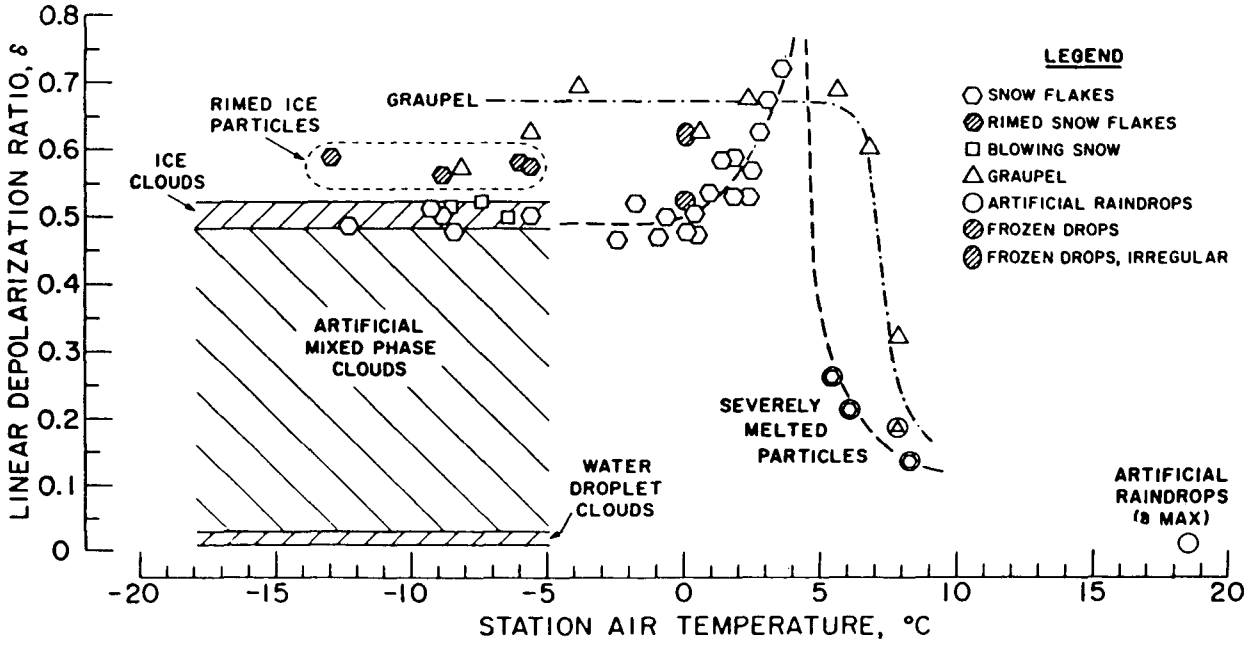

FIG. 3. A compilation of δ values derived from a variety of laboratory and field studies of hydrometeors using the CW laser/lidar analog approach (from Sassen 1976a).

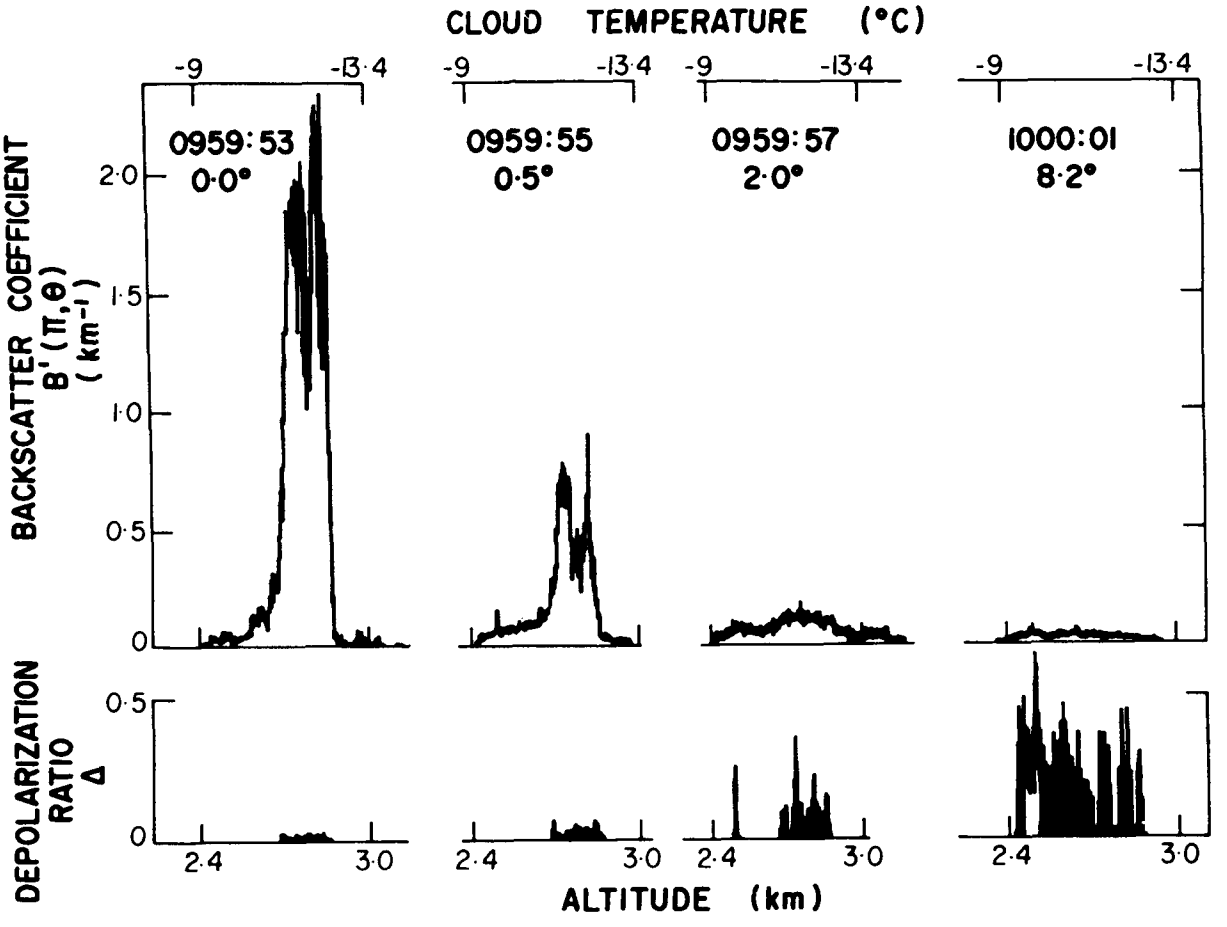

FIG. 4. Lidar field data (from Platt et al. 1978) showing the considerable decrease in planar crystal backscattering (in terms of the backscatter coefficient β') and increase in linear depolarization (Δ used here) as the lidar is scanned off the vertical direction (note the inserted times and lidar angles from the vertical direction). The cloud temperatures are within the expected range for plate crystals, and an aerial sighting of a subsun confirmed their uniform horizontal orientations.

vealed by fields of uniform depolarization ratios (Sassen et al. 1989a), it is clear that polarization lidar is uniquely suited for their study. Although largely overlooked in earlier research, cirrus clouds are a particularly important and yet vaguely described component of the cloud/climate system. A long-term climatological assessment of their depolarization properties was reported by Platt and Dilley (1981) and Platt et al. (1987), among a series of papers describing a range of active and passive cirrus remote-sensing studies. As Fig. 7 (left) shows, average lidar depolarization was found to vary significantly with midcloud temperature in midlatitude cirrus. Along with changes in other scattering parameters, there were indications of a transition in behavior occurring at ~–40°C. This temperature marks a major discontinuity in cloud microphysical processes, so it seems plausible that the effects of supercooled cloud droplets, combined with the shapes of the ice crystals nucleated from them, are being revealed by this extensive dataset. The dashed line in Fig. 7 (left) represents a branching trend in the data collected during winter, which appear to be particularly influenced by such microphysical effects on cirrus cloud content. To further complicate the pattern, tropical cirrus with midcloud temperatures between –50° and -75°C yielded contrasting $\Delta \cong 0.3$ [see Fig. 7 (right)], for reasons that remain obscure. Despite the usefulness of this average picture for climate research, however, cirrus case-study analyses using vertically and temporally resolved δ profiles have revealed more intimate details of cirrus cloud content and behavior.

These cirrus case studies, which were studied not only by lidar but often also with short-wavelength (K-band) radar and aircraft platforms, revealed some interesting properties of cirrus clouds. Perhaps the most surprising was the propensity of cirrus to form with the aid of highly supercooled liquid clouds (Sassen et al. 1985, 1989a, 1990a; Takeda and Horiguchi 1986). The example in Fig. 8 shows lidar depolarization and radar-reflectivity RHI displays (top) collected during an elevation angle scan approximately along

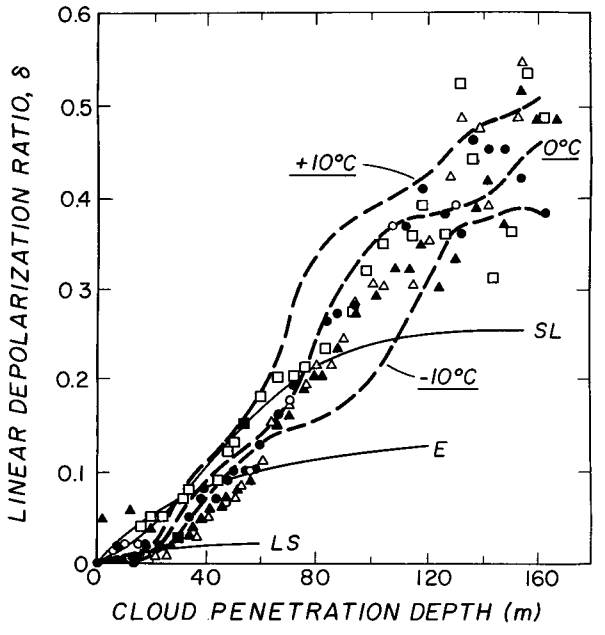

FIG. 5. Comparison of the depolarization generated by cloud-droplet multiple scattering as a function of distance above cloud base from field measurements [the symbols, from four lidar stratus cloud profiles reported by Pal and Carswell (1973)]; the generic water-cloud theoretical predictions of Liou and Schotland (1971; labeled LS), Eloranta (1972; E), and Sun and Li (1989; SL); and the tailored simulations of Sassen et al. (1991) (dashed lines for the three indicated cloud-base temperatures). Figure originally from Pal and Carswell (1973), and subsequently reproduced by Sun and Li (1989) and Sassen et al. (1991).

the heading of an instrumented aircraft leg (at the height indicated by the dashed line), along with the in situ measurements of vertical air velocity W and the concentrations of the detected cloud droplets and ice crystals. Highly supercooled water is indicated by the very low $\delta \leq 0.05$ (the filled-in regions) and $\delta \leq 0.15$ values along the base of the cirrus wave cloud, and confirmed by aircraft measurements at temperatures as low as –35.5°C, the lowest supercooled-liquid temperatures yet reported from in situ measurements. The cloud microphysical model simulation of the glaciation of the liquid bottom layer in Fig. 9 (note the gradual increase in δ above cloud base) aided in the estimation of the homogeneous nucleation rate for the cirrus cloud droplets (Sassen and Dodd 1988). As further illustrated below, this combined empirical/model approach offers considerable promise.

Additional lidar measurements of cirrus clouds showed surprisingly high depolarization at the 10.6-μm CO_2 laser wavelength (Gross et al. 1984), where the strong ice infrared-energy absorption should have inhibited the importance of depolarizing internal reflections. More recent CO_2 lidar observations, however, collected during the NOAA CLARET field experiments, have indicated considerably less cirrus-cloud depolarization (Eberhard, personal communication, 1991). Also quite recently, combined lidar and corona photograph analyses revealed the presence of relatively cold (≤–60°C) cirrus composed of small (≤30-μm

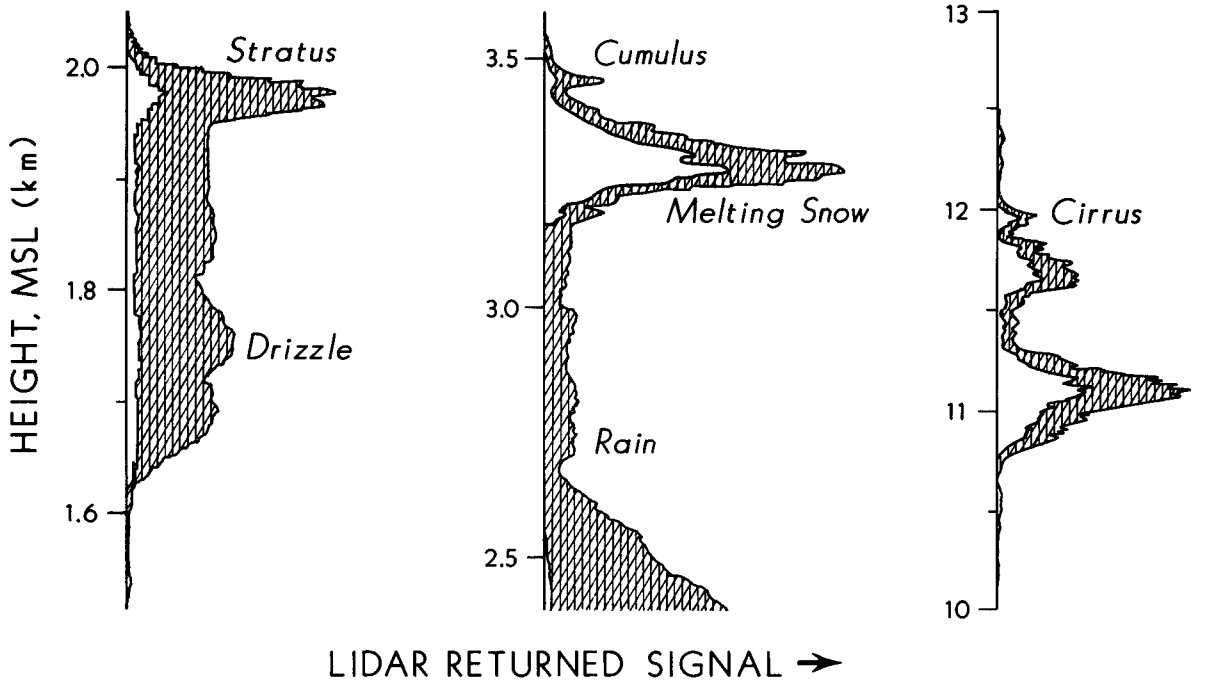

FIG. 6. Dual-channel lidar power profiles (the shaded regions separate the stronger parallel from the orthogonal returns) from three fundamentally different precipitation-particle-generating mechanisms, including, from left to right, drizzle from marine stratus clouds, thunderstorm rainfall from melting snow, and cirrus ice crystal precipitation.

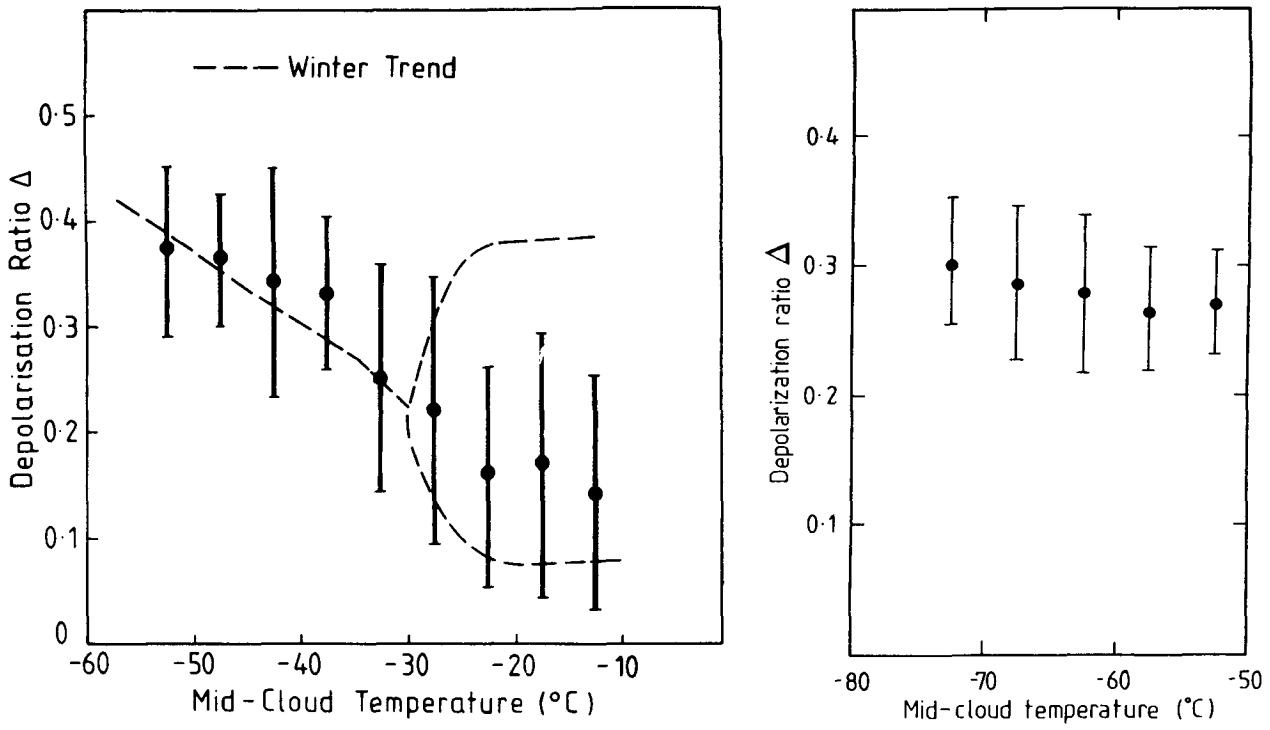

FIG. 7. Schematic diagrams showing the dependence of the vertically integrated linear depolarization ratio (i.e., $\Delta = \Sigma P_\perp / \Sigma P_\parallel$) on midcloud temperature from a large sample of midlatitude (left) and tropical cirrus (from Platt et al. 1987). The mean values and standard deviations in 5°C temperature intervals are shown by the dots and bars. The indicated branching trend in the midlatitude cirrus winter data (dashed lines) is thought to be caused by oriented plate crystal or supercooled cloud-droplet effects.

diameter) ice crystals near the tropopause (Sassen et al. 1989b; Sassen 1991a). The corona-producing ice crystals also yielded unusually high 0.5–0.8 δ values (Sassen 1991a), indicative of some type of ice crystal habit in these extremely cold cirrus. The possible importance of relatively small cirrus ice particles to radiative transfer, as evaluated on the basis of lidar, and satellite or overflying airborne radiative measurements, was explored by Platt et al. (1989), Minnis et al. (1990), and Spinhirne and Hart (1990). There is also evidence from lidar (Sassen et al. 1989a) and numerical (Sassen and Dodd 1989) studies that the radiative effects of haze particles may have to be taken into consideration in cold (≤–40°C) cirrus clouds. Obviously, this is an area that requires further study, and it is apparent that polarization lidar could be quite important in this endeavor.

The basic utility of the polarization-lidar technique (i.e., water- and ice-cloud discrimination) was widely exploited in research of the clouds of the middle and lower troposphere. A fortuitous study of aircraft-produced ice particles (APIP) in a highly supercooled altocumulus cloud, which produced effects similar to those of dry-ice seeding in supercooled water clouds, was encountered during the 1986 Project FIRE cirrus experiment (Sassen 1991b). The lidar relative returned power and depolarization height-time-indicator (HTI) displays of Fig. 10 depict the disruption in the altocumulus layer at ~1955 UTC caused earlier by the performance of the NCAR King Air aircraft mission (the dashed lines). The "seeding" effect was revealed as the cloud drifted overhead by the brief but abrupt decrease in lidar backscattering and the corresponding increase in depolarization in the layer between ~7.5- and 8.1-km altitude. The lidar displays also at times show the presence of an overlying cirrus cloud above ~8.5 km, and oriented planar ice crystals in the virga below the altocumulus (between –17° and –22°C). Times when the lidar was tipped by more than 2° from the zenith are indicated by the "•" symbols below the displays, showing the expected changes from the anisotropic scattering medium.

The unambiguous discrimination of cloud phase is a key measurement capability in winter mountain-storm cloud-seeding research, where it is of paramount importance to identify the locations of embedded supercooled-liquid clouds that could be exploited to yield enhanced precipitation on the barrier. In relation to the capabilities of K-band radar to sense ice crystals, and dual-channel passive microwave-radiometer observations to determine path-integrated liquid water depths, polarization lidar was shown to be an

effective and complementary tool to spatially locate the liquid clouds related to, or decoupled from, natural precipitation production (Sassen 1984). Such multiple remote-sensor measurements describing the climatological (Sassen 1985) and spatial (Sassen et al. 1986) distributions of supercooled liquid water clouds were reported for the Tushar Mountains of southwestern Utah. Figure 11 depicts the relationship between lidar-detected liquid cloud-base temperatures (obtained with the aid of radiosonde data) and concurrent microwave radiometric liquid water depths in Colorado and Utah winter mountain storms. This simple dual-remote-sensor intercomparison illustrates the action of basic cloud processes relating the abundance of supercooled liquid water to the temperature dependencies in the adiabatic release of water, and ice-phase nucleation and water vapor competition effects. In the storm case study described in Sassen et al. (1990b), the relative importance of local orographic, mesoscale, and synoptic-scale processes in generating supercooled liquid clouds and precipitation was explored on the basis of the state-of-the-art multiple remote-sensing approach. An important applied research finding from the Utah mountain studies was that the low-level orographic liquid clouds identified by the lidar appeared to be good cloud-seeding candidates, but the favorable conditions depended on the survival of the liquid in the face of precipitation generated from higher atmospheric levels.

A multiple remote-sensor dataset collected from an orographically dominated stage of a winter storm is provided in Fig. 12. The lidar displays reveal a gradually lowering liquid cloud layer over the mountain barrier with classic depolarization and returned power signatures. Increasing liquid water depths (LW) were concurrently detected passively by a collocated dual-channel microwave radiometer (bottom panel). The K_a-band radar-reflectivity display shows a detached altostratus layer and the lower orographic cloud component (the dashed line indicates the lidar-measured cloud base). The snowshowers that occurred around 0000 and 0400 UTC were categorized by a microphysical observer at the site. Although both showers produced maximum precipitation rates of 0.2 mm h^{-1}, they were composed of different types of ice particles. The first shower was dominated by heavily rimed

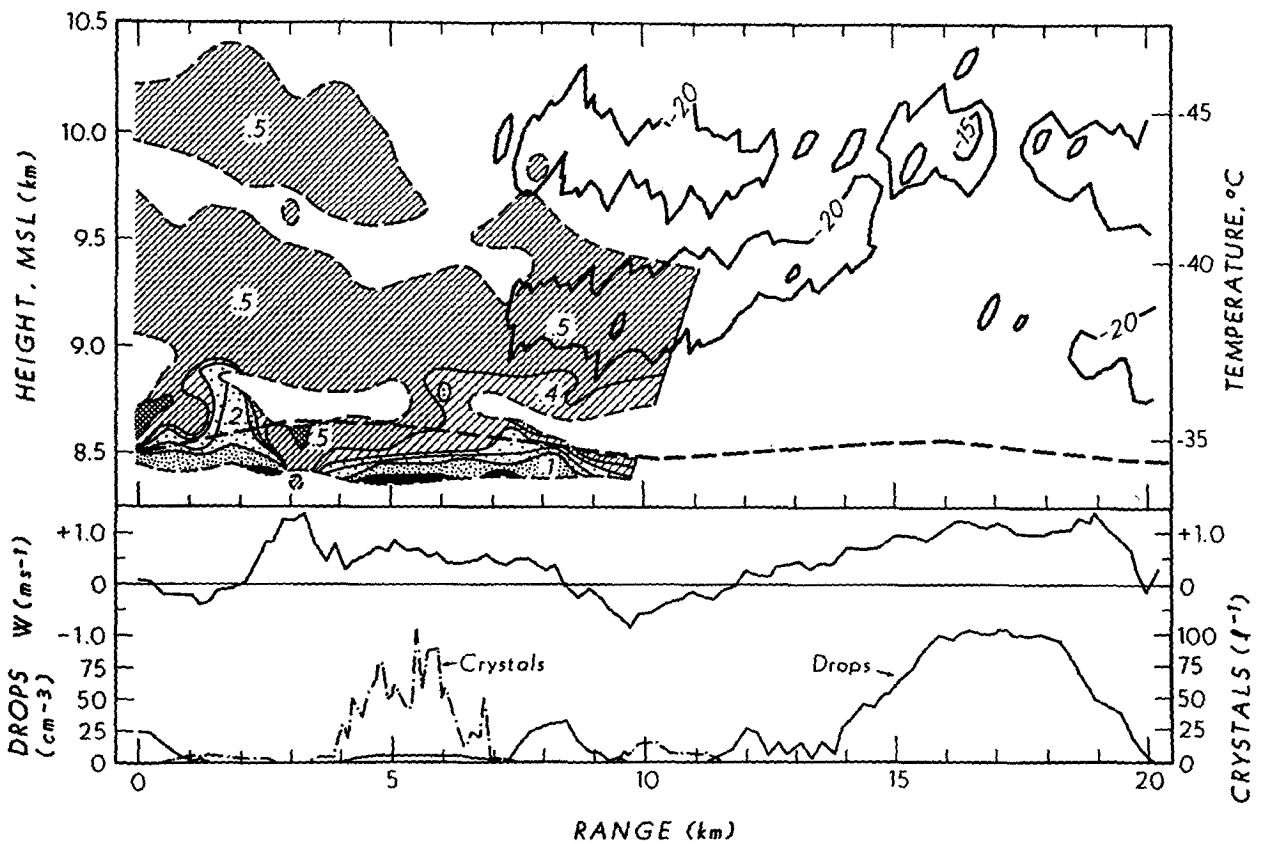

FIG. 8. Range-versus-height displays of partially overlapping elevation angle scans showing lidar δ values (shaded, from 90° to 30°) and C-band water-equivalent radar-reflectivity factors (contoured in dBZ, where signals for angles >45° were obscured by ground clutter) from orographic cirrus wave clouds (from Sassen et al. 1989a). Bottom panels show coordinated vertical velocity W and microphysical data sampled by the NCAR Saberliner, confirming the presence of highly supercooled cirrus cloud droplets at cloud-base locations.

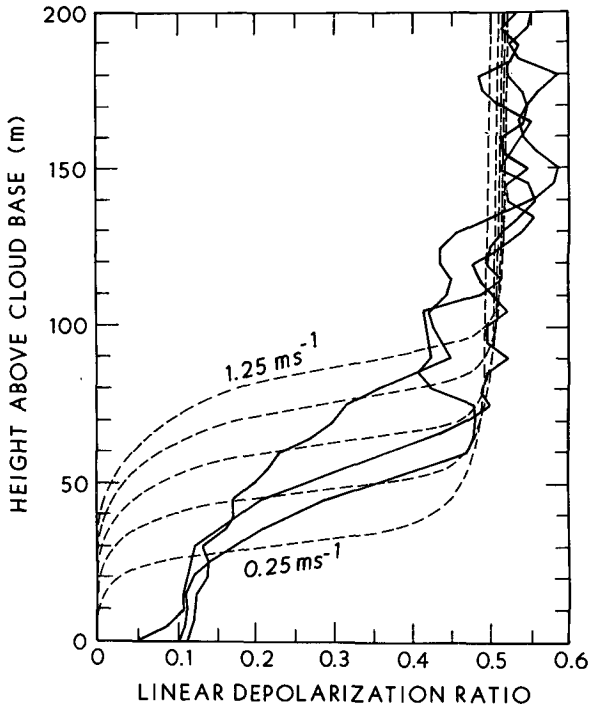

FIG. 9. Mixed-phase cloud model simulations of δ profiles caused by the homogenous freezing of highly supercooled (–35.2°C cloud-base temperature) cirrus cloud droplets (at vertical velocities between 0.25 to 1.25 m s^{-1}, in 0.25-m s^{-1} intervals) compared with representative lidar data (solid lines), after Sassen and Dodd 1988. These model predictions, which neglected the droplet multiple scattering and precipitating ice crystal effects on depolarization of importance near cloud base, nonetheless yielded reasonable agreement in the homogenous droplet freezing rate obtained using other research approaches.

graupel-like particles and the second by mostly lightly rimed dendritic crystals, agreeing well with the ~0.6 to 0.5 decrease in lidar δ values in the precipitation. Also note that the δ values just above the base of the liquid cloud increase during the showers, apparently in response to the increased ice content.

The persistent problem area of accounting for lidar multiple scattering received additional but not conclusive theoretical and experimental attention. The effects of multiple scattering in comparatively diffuse cirrus clouds, which may not noticeably affect depolarization but are nonetheless of considerable importance, were for the first time treated numerically by Platt (1981) and Sun et al. (1989). Lidar depolarization in water clouds was simulated by Cai and Liou (1981) and Sun and Li (1989) using different approaches and yielding divergent results. In the laboratory, the fundamental cause of backscatter depolarization was illustrated by demonstrating the azimuthal polarization anisotropy of single scattering in cloud-droplet assemblies (Carswell and Pal 1980; Pal and Carswell 1985). In the field, Sassen and Petrilla (1986) addressed the lidar operational factors that affect the detection of multiple-scattering-induced depolarization in marine stratus clouds. In addition to evaluating the effects of receiver field-of-view, transmitter/receiver alignment, and lidar elevation angle, the cloud microphysical changes induced by stratus dissipation were shown to cause considerable δ value variability (see Fig. 13). In view of this complicated behavior, it was indicated that

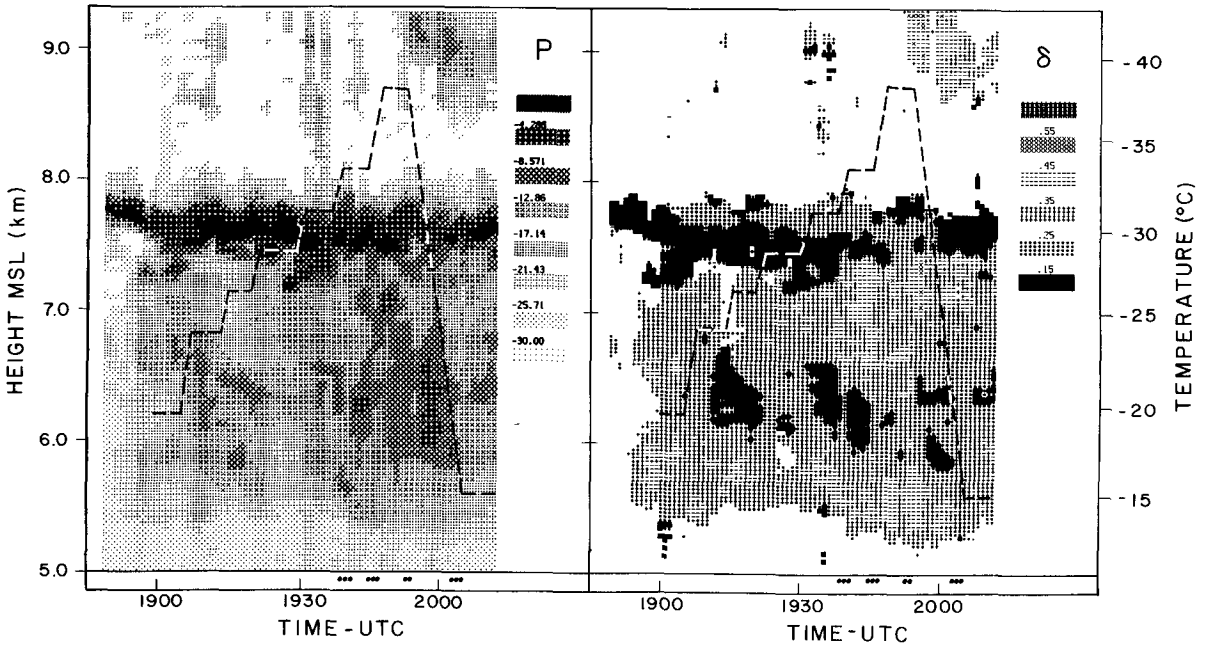

FIG. 10. Height-versus-time displays of relative parallel-polarized returned power (left, shaded in –4.285-dB intervals of the maximum signal) and linear depolarization ratio (right, see δ symbol key) from a highly supercooled (~–30°C) altocumulus layer producing a ~2-km-deep virga layer. Dashed lines give the supporting aircraft flight altitudes in the vicinity of the lidar ground site.

lidar depolarization data could have value in the remote sensing of stratus cloud structure and composition.

This section can not be concluded before discussing an application that amply illustrated the remote-sensing capabilities of the technique, and, at the same time, showed the feasibility of advanced lidar technologies. This significant development involved the deployment of polarization lidar on high-flying NASA ER-2 aircraft (Spinhirne et al. 1982), a highly mobile platform. This system was applied to the research of cumuliform cloud systems in Florida and Montana (Spinhirne et al. 1983), marine stratus off the California coast (Spinhirne et al. 1989), and midlatitude cirrus (Heymsfield et al. 1990; Sassen et al. 1990a; Spinhirne and Hart 1990). Figures 14 and 15 provide outstanding examples of the research findings. It is clear that the essentially Eulerian view provided by such downward-looking observations represents a highly useful application of the polarization-lidar technique. Hopefully, such usage foreshadows spaceborne applications.

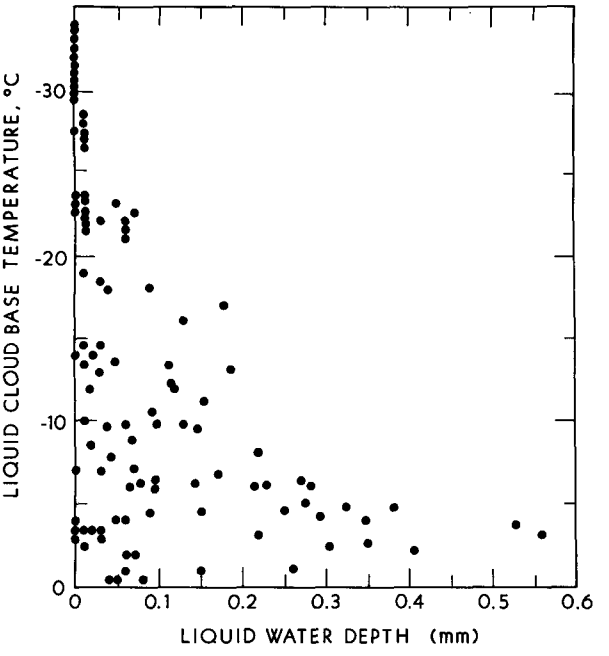

FIG. 11. Dual remote-sensor intercomparison of lidar- and radiosonde-derived orographic liquid cloud-base temperature, and dual-channel microwave-radiometer liquid water depths, after Sassen 1985 (with additional data points from Sassen et al. 1990b). The data reveal the action of fundamental mixed-phase cloud adiabatic processes, and also show the surprising extent of liquid cloud supercooling temperatures in winter mountain storms.

4. Current prospects and problems

It has been apparent for over two decades that a drawback to the application of the polarization-lidar technique is the lack of a working theory to simulate and help interpret the returned energy and depolarization profiles obtained from atmospheric clouds. Conditions of little concern to traditional radar measurements, including multiple scattering, propagation, and non-Rayleigh nonspherical scattering effects, are of great importance to lidar cloud studies. Fortunately, significant improvements in our ability to treat the optical scattering behaviors of hydrometers, including depolarization, are promised to be forthcoming. Recent developments in simple hexagonal ice-crystal scattering theory based on the geometrical optics ray-tracing approach (Takano and Jayaweera 1985; Takano and Liou 1989) display the potential for permitting ice crystal habit (i.e., axial ratio) identification and eventually treating the more complex particle shapes that are commonly found in cirrus and precipitation, to establish the foundations for a more viable lidar theory. Although it remains necessary to generate ray-tracing results that are consistent with realistic cloud contents (in a quite different manner than microwave relations are inferred from particle-size distributions), encouraging initial steps at interpreting lidar cirrus cloud measurements have been based on preliminary theoretical findings (Sassen et al. 1989b).

Another area of lidar research with indicated potential is based on the application of sophisticated cloud microphysical models to predict the composition and corresponding optical backscattering properties of various clouds. Beginning with quite simple models (Sassen 1977b,c), this field has progressed to more detailed simulations of cirrus clouds (Sassen and Dodd 1988, 1989), which rely on combining empirical ice-particle and Mie-theory droplet-scattering properties. An area of current concern is the interpretation of polarization-lidar returns from mixed water- and ice-phase clouds, which comprise a significant proportion of deep-convective, winter-storm, and altocumulus clouds, as well as some cirrus. Previously, it has not been possible to separate the depolarized contributions from cloud-droplet multiple scattering and ice-particle single scattering. Figure 16 provides examples of typical lidar returned power and δ value profiles through a precipitating supercooled orographic liquid cloud. For comparison, results from our current program to evaluate the depolarizing properties of similar mixed-phase clouds are given in Fig. 17.

The field data in Fig. 16 show a supercooled (~–8°C) liquid cloud emerging from snowfall returns during a winter storm over the Tushar Mountains. According to K_a-band radar data, the snowfall was generated at higher levels and decreased rapidly in intensity over this 30-min period (i.e., ice equivalent radar-reflectivity factors near the surface dropped from about 5 to –15

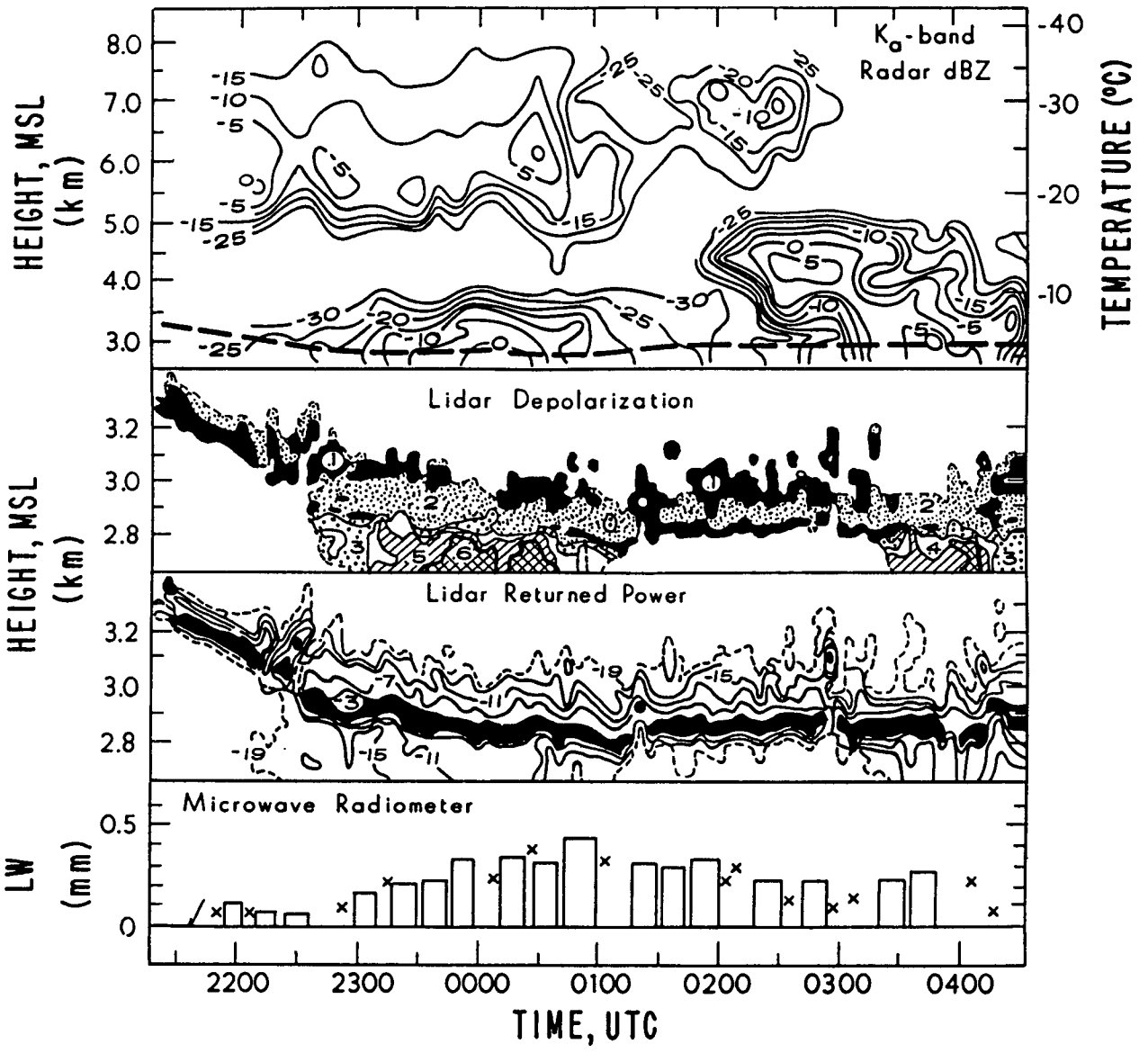

FIG. 12. A multiple remote-sensor dataset from a winter mountain storm showing, from top to bottom, height-versus-time k_a-band radar-reflectivity factor and lidar depolarization and relative returned-power displays, and zenith normalized dual-channel microwave-radiometer liquid water (LW) depths for intermittent zenith (X symbols) and 360°-azimuth scan-averaged (bars) data. The sensitivities of the various instruments, and their complementary nature, are well illustrated by this dataset (modified from Sassen et al. 1990b).

dBZ). The lidar data illustrate the concurrent appearance of a gradually descending liquid cloud layer not far above the midbarrier field site (2.56 km above sea level). The liquid cloud base is clearly marked by abrupt signal increases and depolarization decreases to $\delta < 0.15$, before strong attenuation and droplet multiple-scattering δ-value increases become evident aloft. In contrast, δ values in the snowfall below the orographic cloud are mostly in the 0.35–0.5 range.

The mixed-phase cloud model simulations of Fig. 17 are based on the general cloud properties encountered in Tushar Mountain winter storms under such conditions, and the operational features of our lidar system. The one-dimensional model has been described in Sassen and Dodd (1988, 1989), but in the present case an analytical treatment of multiply scattered energy and droplet depolarization in the lidar receiver beamwidth are included. The special form of the lidar equation used to prescribe the backscattered powers P_r in the parallel, II, and orthogonal, $\perp$, polarization planes from water w and ice i particles, as a function of range R, is given by,

$$P_r(R)_{\parallel,\perp} = \frac{k}{R_2}\,[\beta'_w(R)_{\parallel} + \beta'_i(R)_{\parallel,\perp} + \beta_w(R)_{\parallel,\perp}) \exp -2\int_{R_1}^{R_2} (\eta_w(R)\,\sigma_w(R) + \eta_i(R)\,\sigma_i(R)]\,dR, \quad (1)$$

where k is the lidar system constant, β and σ the volume backscattering and extinction coefficients, and η a forward multiple-scattering correction factor. The primary backscattering coefficients are identified by the primes, leading to the following definition for the mixed-phase cloud linear depolarization ratio:

$$\delta(R) = \frac{\beta'_i(R)_\perp + \beta_w(R)_\perp}{\beta'_i(R)_\parallel + \beta'_w(R)_\parallel + \beta_w(R)_\parallel}. \quad (2)$$

The droplet multiple-backscattering coefficients $\beta_w(R)_{\parallel,\perp}$ are based on azimuthally integrated Mie-theory single-scattering phase functions (Sassen and Petrilla 1986) for the evolving droplet size distribution, and the probability of detecting double backscattering based on purely geometric concerns. Although a detailed description of the model will be reported elsewhere (Sassen et al. 1991), a comparison of our predictions for pure liquid clouds (dashed lines) with the measurements given in Fig. 5 indicates that our approximate treatment of multiple-scattering depolarization has noticeable advantages over previous theoretical attempts (the solid lines).

Although the rate of depolarization increase generated by droplet multiple scattering is a function of a number of factors, it is basically the sizes of the droplets and the volume of the cloud viewed by the receiver that controls the process. Keeping lidar operational and cloud thermodynamic (e.g., temperature and updraft velocity) factors constant, a change in ice content will modulate the droplet-size distribution through droplet/crystal water vapor competition effects, thereby affecting the generation of depolarization. In Fig. 17 (see caption for model input parameters), changes in lidar returns caused by the ventilated growth of 500-μm-long column crystals (with 2:1 axis ratio) are shown as a function of ice crystal concentration. (For simplicity, the precipitating ice particles are not allowed to increase in size between time steps or scavenge cloud droplets through the riming process.) The relative parallel-polarized returned power and δ profiles are shown as the background crystal concentration N_i is decreased from 20 to 0 l^{-1}. Note that the increase in the cloud peak signal reflects both the decrease in attenuation due to precipitation below cloud base and the increase in cloud-

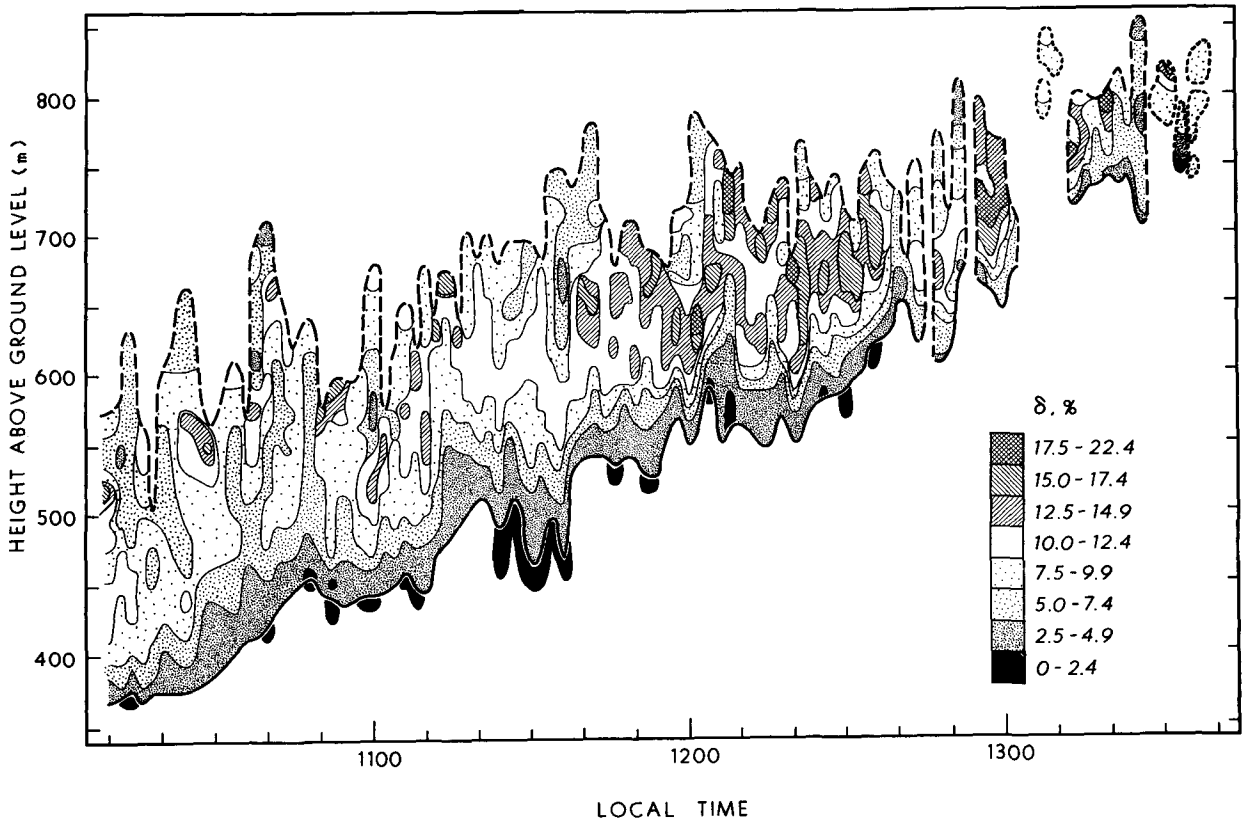

FIG. 13. Height-versus-time display of lidar linear depolarization (see key) measured during the dissipation (with solar heating) of a marine stratus cloud advected by onshore winds along the southern California coast. The solid line marks the cloud base (with occasional drizzle returns below); the heavy dashed line, the apparent (attenuation-limited?) cloud top; and the short-dashed lines, the depolarized aerosol returns left behind by cloud evaporation. Compared with the field data in Fig. 5, obtained using larger lidar beamwidths, it is clear that 1-mrad beamwidths can restrict multiple-scattering δ values to relatively innocuous levels.

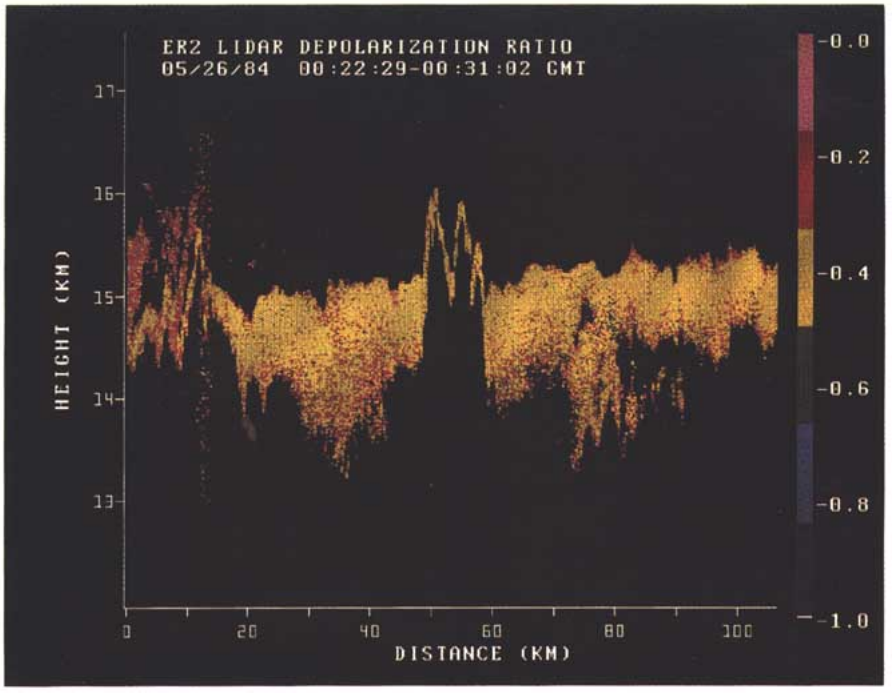

FIG. 14. Airborne (downward-pointing) polarization-lidar height-versus-distance δ value display (note color key) obtained from the NASA ER-2 over southern Illinois at the indicated date and time, showing a dense (attenuation-limiting) thunderstorm top protruding through more tenuous cirrus at 50–60-km distance. Despite the differences in optical thickness (the thin tropopause cirrus layer was not visible in the data from the imaging radiometers aboard the ER-2), relatively uniform $\delta \cong 0.5$ are present throughout. (Figure courtesy of J. D. Spinhirne.)

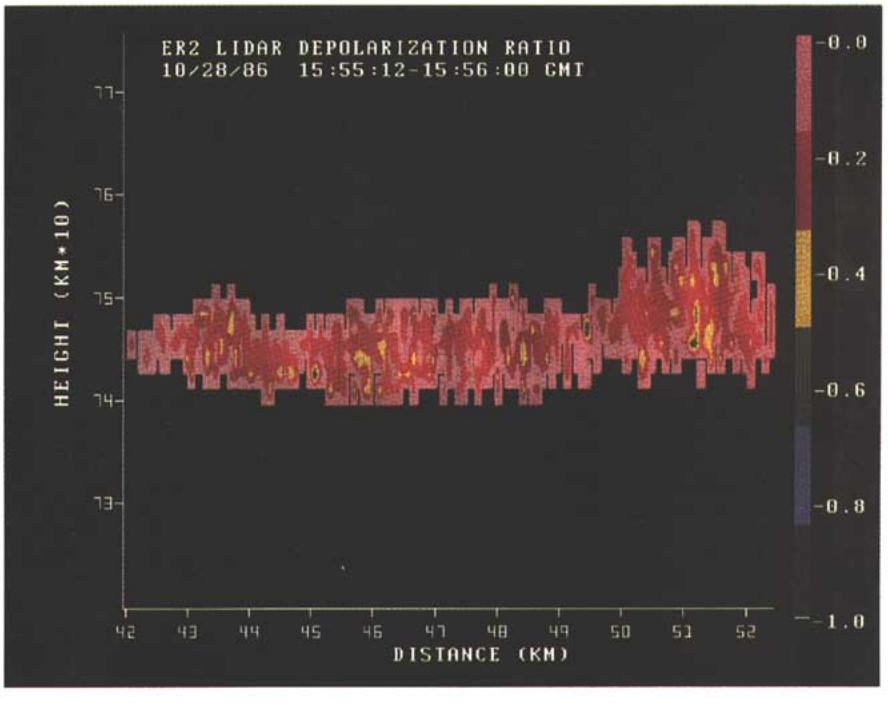

FIG. 15. An expanded view of a highly supercooled (~–30°C) altocumulus cloud obtained from the ER-2 platform (as in Fig. 14) over central Wisconsin during Project FIRE (see also Heymsfield et al. 1991). Ground returns were generally recovered through this optically thin water cloud, and significant increases in multiple-scattering-induced depolarization are confined to the denser cellular structures. Note that the height scale should be divided by 10. (Figure courtesy of J. D. Spinhirne.)

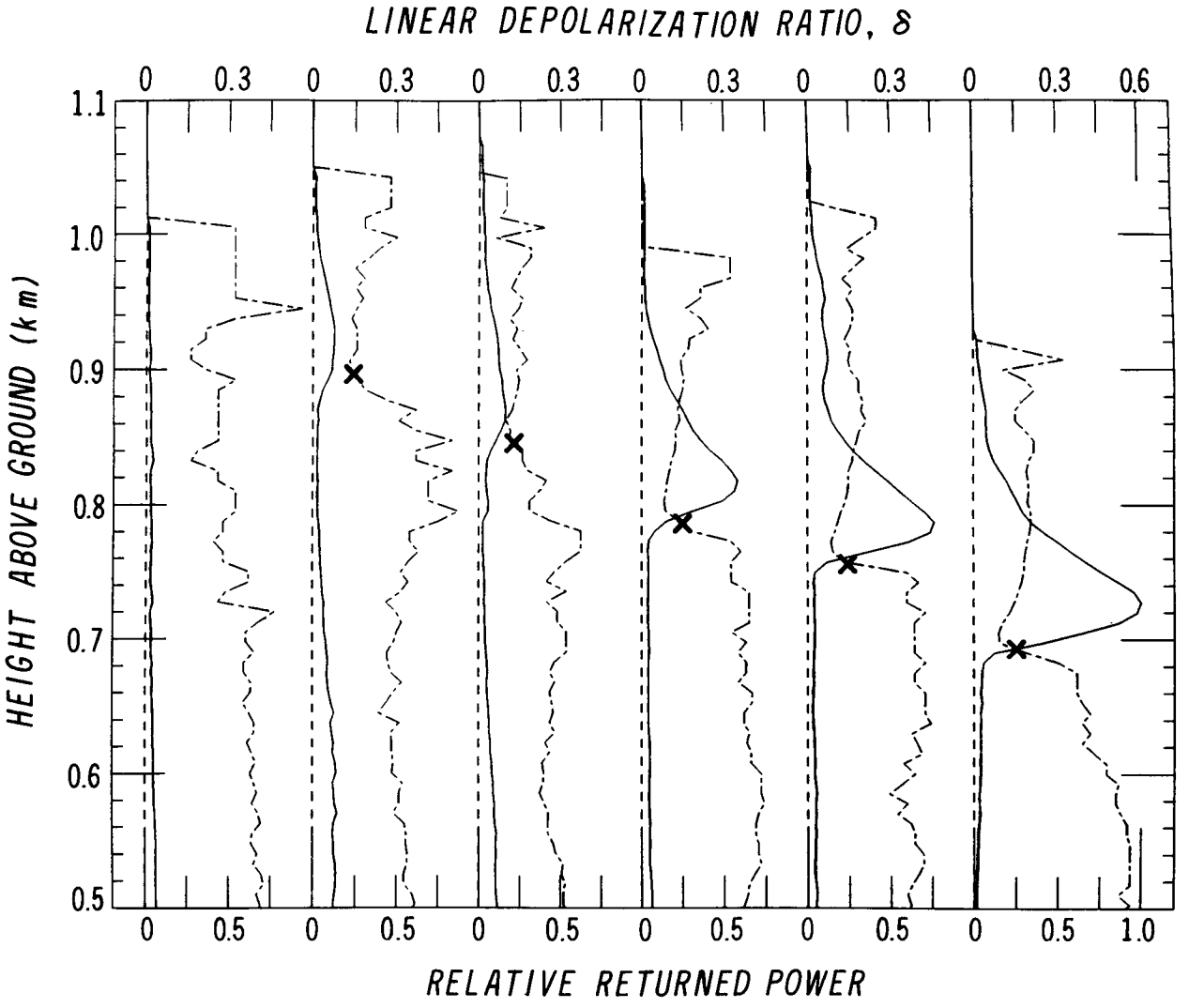

FIG. 16. Polarization-lidar relative returned-power (solid, normalized to the maximum peak at right) and δ-value (dashed) profiles obtained on 10 February 1987 from a winter mountain storm, showing the emergence of a supercooled orographic liquid cloud layer as the snowfall intensity decreased. "x" symbols mark where δ first decline to 0.15, a basic criterion used to locate liquid-dominated cloud bases in winter storm clouds. The height resolution of this unaveraged data is 7.5 m.

base water content with decreasing ice-phase competition. The depolarization profiles reveal that the minimum cloud base δ decreases, but, surprisingly, the maximum δ in the cloud (at the height where $P_r(R)_{\parallel}$ declines to simulated noise-dominated levels) tends to increase with decreasing ice content.

Comparison of Figs. 16 and 17 suggests that such theoretical approaches are valuable for evaluating the cloud-research potential of polarization techniques and interpreting field data. Although a duplication of the observed dataset was not intended, it is indicated that the complex microphysical processes occurring in mixed-phase clouds can be brought under scrutiny using this largely unexplored combined remote-sensing/cloud-model approach. Despite the use of the arbitrary model inputs and the simplified treatment of ice particle effects, the generic orographic cloud-model predictions and typical field data are basically similar, and even reproduce the gradual liquid cloud-base height variations often observed during periods of variable snowfall (Sassen et al. 1990b). It should be stressed, however, that the utility of this approach can be significantly enhanced by the availability of supplemental in situ or remote-sensing information to define unknown data quantities. For example, Fig. 18 illustrates the effects of varying the updraft velocity *U* on the mixed-phase cloud simulations. It can be seen that, keeping other factors constant, a decreasing vertical velocity also affects the cloud-base height and the δ profiles by increasing the importance of ice-

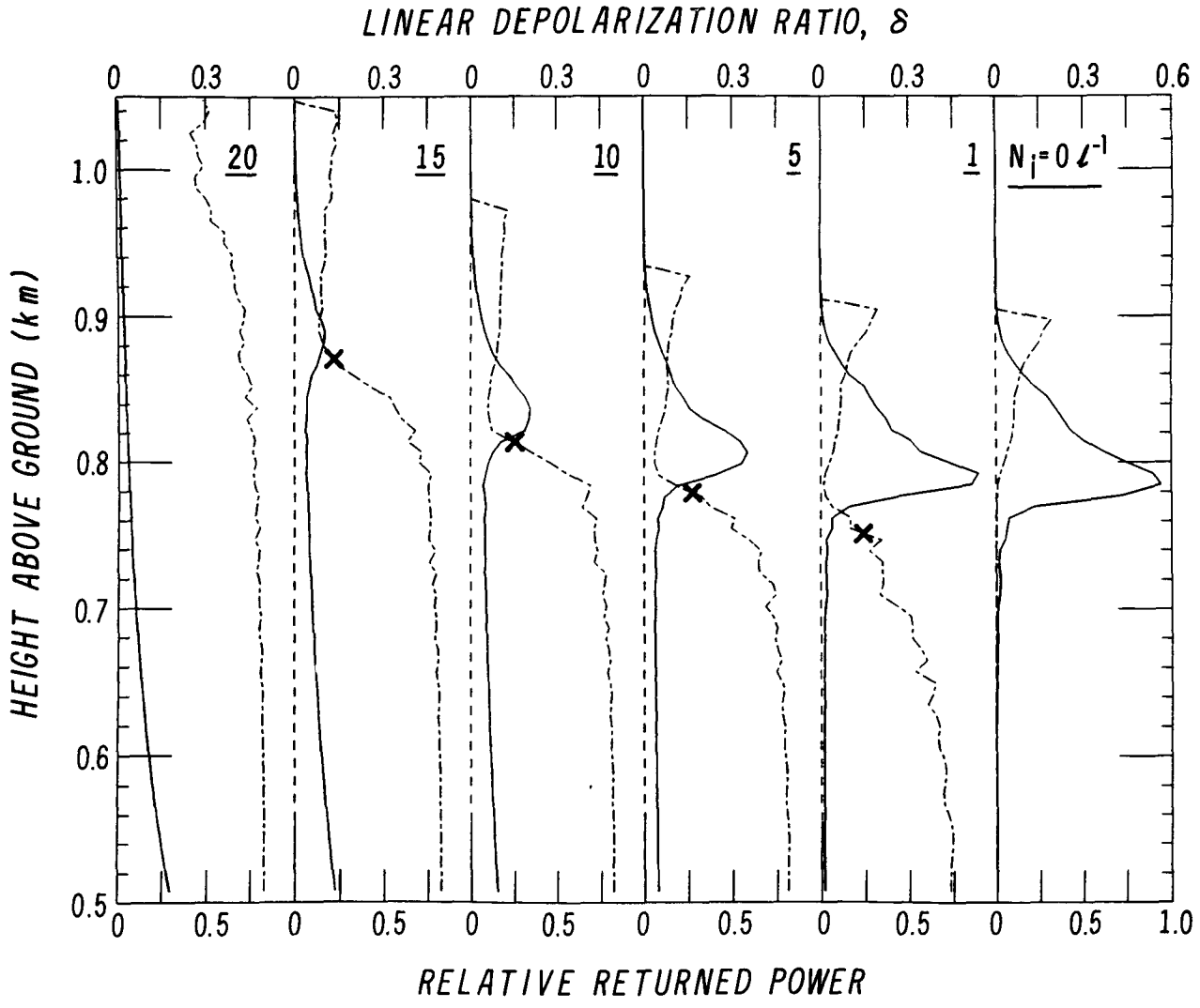

FIG. 17. Mixed-phase cloud microphysical model simulations based on conditions similar to those in Fig. 16, examining the returned-power and δ-value profiles (as in Fig. 16) from single droplet and ice crystal, and multiple droplet backscattering, as a function of the indicated background ice-crystal concentration N_i. Model inputs are vertical velocity 0.5 m s^{-1}, droplet concentration 200 cm^{-3}, and ice-column length 500 μm. The simulations are initialized at −10°C, a 750-mb pressure, an 85% relative humidity, and a 500-m height above ground in each case.

phase water vapor competition results. Similar results are produced by increasing either the ice crystal size or concentration.

5. Conclusions and outlook

In this paper, frequent use has been made of analogies between the development and application of "weather" radar and lidar systems. This has served the dual purpose of acknowledging the pioneering of basic remote-sensing principles by radar researchers and tracing important parallel developments in the polarization lidar field. Initially, it appeared that lidar techniques, with their depth-of-probing limitations, all-weather field reliability problems, and lack of nonspherical-particle-scattering–theory support, would remain in the shadow of microwave radar.[2] However, it is (hopefully) now apparent that polarization lidar offers important atmospheric remote-sensing measurement capabilities that are fundamentally different from those of radar and other sensors, and is particularly valuable as part of a multiple-remote-sensor approach. In essence, the strong interaction of laser

[2] To quote a leading radar researcher prior to a lidar lecture given at McGill University in December 1976: "So you're one of those fellows who prefer to use lasers instead of microwaves." Joint radar and lidar conferences have yet to be held.

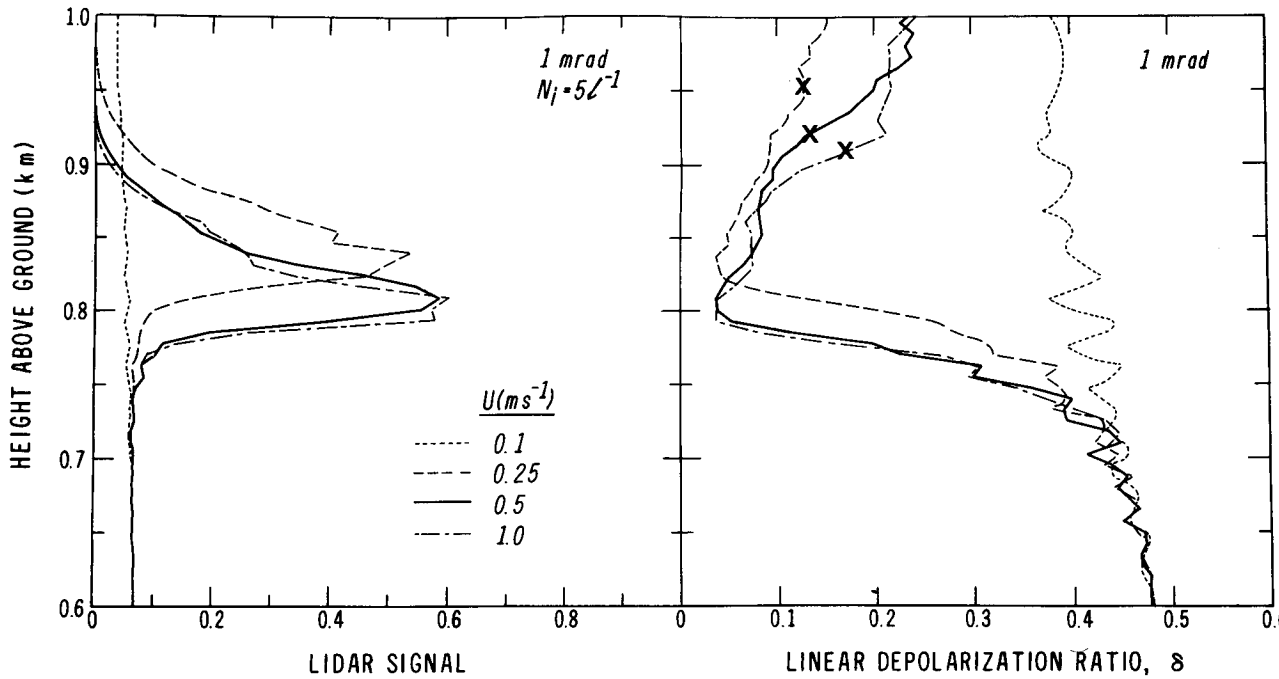

FIG. 18. Model results based on the same inputs as Fig. 17, except that the updraft velocity U is treated as a variable, and the crystal concentration is constant at $N_i = 5\ l^{-1}$. The "x" symbols mark the maximum observable δ values in the attenuated cloud signals, and 1 mrad refers to the matched transmitter/receiver beamwidths modeled. Note that water saturation is not attained at $U = 0.1$ m s^{-1}, due to the comparatively low adiabatic moisture-release rate, although CCN activation/haze particle growth within the (former) liquid cloud region leads to a small δ decrease, a previously unrecognized phenomenon that occurs in winter mountain-storm clouds during snowfall.

light with hydrometeors that leads to the often range-limiting attenuation provides for unparalleled sensitivity to cloud content in those cloud regions accessible to lidar probing. Since visible polarization-lidar provides information similar to that sensed by the human eye (although obviously with the significant advantages of accurate range resolution and scattered-light polarization analysis), lidar research applications and limitations are linked in a curious fashion to the visual perception of our environment, a fact that has no doubt helped direct the development of this field.

Technologically, the future of this field can be expected to benefit from increasingly capable microcomputer systems to handle enhanced multichannel polarization data streams. (As far as the polarization-lidar transmitter is concerned, little improvement has been needed since the advent of the "industrial" visible and near-infrared lasers in the 1970s.) For example, we are currently fabricating as part of the ARM program a polarization-diversity lidar system capable of simultaneous two-color, four-polarization-channel data acquisition at the 10-Hz pulse-repetition frequency of the transmitter. Such data-acquisition capabilities enable complete (one-color) Stokes parameter measurements during scanning or variable field-of-view cloud studies at the maximum PRF. Since it is becoming possible to (relatively inexpensively) characterize the complete backscatter polarization properties of atmospheric targets at high resolution and at multiple wavelengths, it can be said that we are entering a new age of polarization-lidar research. [Earlier, Houston and Carswell (1978) concluded that the two-channel method was "the most efficient way to utilize lidar," since "the additional data handling required for the full four-channel measurements may not be warranted for most atmospheric studies."]

Importantly, it is in the realm of lidar theoretical support that we may expect significant improvements in data-analysis approaches to achieve a broader understanding of the remotely sensed atmospheric conditions. Computer ray-tracing methods are at the threshold of treating more realistic, complex ice-particle shapes, such as the hollow column, bullet rosette, or rimed snowflake. In such particles, scatterings at internal air–ice interfaces and between neighboring crystal elements (a sort of multiple scattering within a particle) will likely dominate the backscattering and alter the angular distribution of scattered light. Furthermore, as illustrated here, the modeling of the detailed microphysical and corresponding optical scattering properties of realistic clouds is certainly a promising approach. It is valuable for both assessing the general information content of lidar measurements and helping to interpret field data to learn more about the cloud properties (as in Figs. 9 and 17). As recently pointed out (Sassen et al. 1991), misleading results were

obtained in previous multiple-scattering depolarization simulations because unrealistic, vertically homogeneous water cloud contents were treated without regard to the adiabatic process. It must of course be acknowledged that any remote-sensing technique has limitations on the range and scope of data quantities that can be derived. For example, our recent model simulations have shown that although a measure of the relative ice–water balance of mixed-phase clouds can be inferred from the δ profile, it is another matter to quantify their mass contents (which depend on several thermodynamic and microphysical variables). In view of these limitations, it is obvious that the information provided by polarization lidar is enhanced by supplemental data from in situ probes or other remote sensors. Even basic supporting (e.g., visual and temperature) observations that help to establish the context of the meteorological conditions being probed can be of great aid in interpreting lidar polarization data, since potential ambiguities can thus be removed from consideration. Polarization lidar has proven to be a particularly useful cloud-research tool when deployed as part of a multiple remote-sensor ensemble, in which the information contents of the instruments at various wavelengths combine synergistically (as in Figs. 11 and 12) and help to eliminate unknowns in the set of remote-sensing equations. At the same time, it should not be overlooked that inherent in the polarization-lidar technique are unique research capabilities, such as unambiguous cloud-phase discrimination and an almost ideal sensitivity to cirrus clouds.

It is probable that the special cloud microphysical sensing capabilities of the polarization-lidar technique will ultimately be exploited from space-based platforms, just as they have been increasingly utilized from aircraft. Spaceborne lidars have long been a goal, and interests in nonmilitary applications are intensifying. As mentioned earlier, the additional hardware needed for two-channel polarization measurements is not prohibitive, and so the significant amount of extra information gained is economical. Global coverage will provide significant insights into the state and composition of the atmosphere, an area of considerable importance to climate research. It is also likely that the clouds of extraterrestrial atmospheres, when subjected to lidar study from suitable platforms, will yield basic measurements of cloud composition. This follows from the fundamental optics principles governing the scattering of light by particles of arbitrary shape, no doubt including the exotic cloud particles of the other planets.

Acknowledgments. The author wishes to acknowledge, in particular, the support of our lidar research program by the National Science Foundation, most recently under Grant ATM-8914348. Current support for FIRE cirrus research is also provided by NASA Grant NAG-1-868; winter mountain-storm and cloud-modeling studies by Utah Division of Water Resources Contract 90-1039 (as part of cooperative weather modification program under NOAA Agreement NA89RAH09090); and advanced polarization-diversity lidar and cloud-identification algorithm development by DOE Grant DE-FG02ER61059 from the ARM Instrument Development Program. The contributions to the current cloud-modeling effort by H. Zhao and G.C. Dodd are gratefully acknowledged, and I thank C. M. R. Platt and J. D. Spinhirne (with the help of D. Hlavka and the support of the NASA Atmospheric Dynamics and Radiation Office) for providing copies of their figures. Finally, I would like to thank R. M. Schotland for encouraging my involvement in this then-incipient field of research.

References

Allen, R.J., and C.M.R. Platt, 1977: Lidar for multiple backscattering and depolarization observations. *Appl. Opt.*, **16,** 3193–3199.

Cai, Q., and K.-N. Liou, 1981: Theory of time-dependent multiple backscattering from clouds. *J. Atmos. Sci.*, **38,** 1452–1466.

Carswell, A.I., 1983: Lidar measurements of the atmosphere. *Canadian J. Phys.*, **61,** 378–395.

——, and S.R. Pal, 1980: Polarization anisotropy in lidar multiple scattering from clouds. *Appl. Opt.*, **19,** 4123–4126.

Cohen, A., 1975: Cloud-base water content measurement using single wavelength laser-radar data. *Appl. Opt.*, **14,** 2873–2877.

Collis, R.T.H., and P.B. Russell, 1976: *Laser Monitoring of the Atmosphere*, E.D. Hinkley, Ed., Springer-Verlag, Berlin.

Derr, V.E., N.L. Abshire, R.E. Cupp, and G.T. McNice, 1976: Depolarization of lidar returns for virga and source cloud. *J. Appl. Meteor.*, **15,** 1200–1203.

Eloranta, E.W., 1972: Calculation of doubly scattered lidar returns. Ph.D. dissertation, U. Wisconsin, Madison, 115 pp. [Available from University of Wisconsin, Madison]

Gross, A., M.J. Post, and F.F. Hall, Jr., 1984: Depolarization, backscatter, and attenuation of CO_2 lidar by cirrus clouds. *Appl. Opt.*, **23,** 2518–2522.

Heymsfield, A.J., K.M. Miller, and J.D. Spinhirne, 1990: The 27–28 October 1989 FIRE cirrus cloud case study: Cloud structure and composition from in situ measurements. *Mon. Wea. Rev.*, **118,** 2313–2328.

——, L.M. Miloshevich, A. Slingo, K. Sassen, and D. O'C Starr, 1991: An observational and theoretical study of highly supercooled altocumulus. *J. Atmos. Sci.*, **48,** 923–945.

Houston, J.D., and A.I. Carswell, 1978: Four-component polarization measurements of lidar atmospheric scattering. *Appl. Opt.*, **17,** 614–620.

Liou, K.-N., 1972: On depolarization of visible light from water clouds for monostatic lidar. *J. Atmos. Sci.*, **29,** 1000–1003.

——, and R.M. Schotland, 1971: Multiple backscattering and depolarization from water clouds for a pulsed lidar system. *J. Atmos. Sci.*, **28,** 772–784.

——, and H. Lahore, 1974: Laser sensing of cloud composition: A backscatter depolarization technique. *J. Appl. Meteor.*, **13,** 257–263.

Minnis, P., D.F. Young, K. Sassen, J.M. Alvarez, and C.J. Grund, 1990: The 27–28 October 1986 FIRE IFO cirrus case study: Cirrus parameter relationships derived from satellite and lidar data. *Mon. Wea. Rev.*, **118,** 2402–2425.

Pal, S.R., and A.I. Carswell, 1973: Polarization properties of lidar backscattering from clouds. *Appl. Opt.*, **12,** 1530–1535.

——, and ——, 1976: Multiple scattering in atmospheric clouds: Lidar observations. *Appl. Opt.*, **15,** 1990–1995.
——, and ——, 1977: The polarization characteristics of lidar scattering from snow and ice crystals in the atmosphere. *J. Appl. Meteor.*, **16,** 70–80.
——, and ——, 1985: Polarization anisotropy in lidar multiple scattering from atmospheric clouds. *Appl. Opt.*, **24,** 3464–3471.
Platt, C.M.R., 1977: Lidar observation of a mixed-phase altostratus cloud. *J. Appl. Meteor.*, **16,** 339–345.
——, 1978: Lidar backscatter from horizontal ice crystal plates. *J. Appl. Meteor.*, **16,** 482–488.
——, 1981: Remote sounding of high clouds. Part III: Monte Carlo calculations of multiply scattered lidar returns. *J. Atmos. Sci.*, **38,** 156–167.
——, and A.C. Dilley, 1981: Remote sounding of high clouds. Part IV: Observed temperature variations in cirrus optical properties. *J. Atmos. Sci.*, **38,** 1069–1082.
——, N.L. Abshire, and G.T. McNice, 1978: Some microphysical properties of an ice cloud from lidar observations of horizontally oriented crystals. *J. Appl. Meteor.*, **17,** 1220–1224.
——, J.C. Scott, and A.C. Dilley, 1987: Remote sounding of high clouds. Part VI: Optical properties of midlatitude and tropical cirrus. *J. Atmos. Sci.*, **44,** 729–747.
——, J.D. Spinhirne, and W.D. Hart, 1989: Optical and microphysical properties of a cold cirrus cloud: Evidence for regions of small ice particles. *J. Geophys. Res.*, **94,** 11 151–11 164.
Ryan, J.S., S.R. Pal, and A.I. Carswell, 1979: Laser backscattering from dense water-droplet clouds. *J. Opt. Soc. Am.*, **69,** 60–67.
Sassen, K., 1974: Depolarization of laser light backscattered by artificial clouds. *J. Appl. Meteor.*, **13,** 923–933.
——, 1975: Laser depolarization "bright band" from melting snowflakes. *Nature*, **225,** 316–318.
——, 1976a: An evaluation of polarization diversity lidar for cloud physics research. Ph.D. dissertation, University of Wyoming, Laramie, 409 pp.
——, 1976b: Polarization diversity lidar returns from virga and precipitation: Anomalies and the bright band analogy. *J. Appl. Meteor.*, **15,** 292–300.
——, 1977a: Ice crystal habit discrimination with the optical backscatter depolarization technique. *J. Appl. Meteor.*, **16,** 425–431.
——, 1977b: Lidar observations of high plains thunderstorm precipitation. *J. Atmos. Sci.*, **34,** 1444–1457.
——, 1977c: Cloud phase discrimination with polarization diversity lidar. *J. Rech. Atmos.*, **11,** 179–190.
——, 1978: Air-truth lidar polarization studies of orographic clouds. *J. Appl. Meteor.*, **17,** 73–91.
——, 1980: An initial application of polarization lidar for orographic cloud-seeding operations. *J. Appl. Meteor.*, **19,** 298–304.
——, 1984: Deep orographic cloud structure and composition derived from comprehensive remote-sensing measurements. *J. Climate Appl. Meteor.*, **23,** 568–583.
——, 1985: Supercooled liquid water in winter storms: A preliminary climatology from remote sensing observations. *J. Wea. Mod.*, **17,** 30–35.
——, 1991a: Corona-producing cirrus cloud properties derived from polarization lidar and photographic analyses. *Appl. Opt.*, **30,** 3421–3428.
——, 1991b: Aircraft produced ice particles in a highly supercooled altocumulus cloud. *J. Appl. Meteor.*, **30,** 765–775.
——, and R.L. Petrilla, 1986: Lidar depolarization from multiple scattering in marine stratus clouds. *Appl. Opt.*, **25,** 1450–1459.
——, and G.C. Dodd, 1988: Homogeneous nucleation rate for highly supercooled cirrus cloud droplets. *J. Atmos. Sci.*, **45,** 1357–1369.
——, and ——, 1989: Haze particle nucleation simulations in cirrus clouds, and applications for numerical and lidar studies. *J. Atmos. Sci.*, **46,** 3005–3014.
——, K.N. Liou, S. Kinne, and M. Griffin, 1985: Highly supercooled cirrus cloud water: Confirmation and climatic implications. *Science*, **227,** 411–413.
——, R.M. Rauber, and J.B. Snider, 1986: Multiple remote sensor observations of supercooled liquid water in a winter storm at Beaver, Utah. *J. Climate Appl. Meteor.*, **25,** 825–834.
——, D.O'C. Starr, and T. Uttal, 1989a: Mesoscale and microscale structure of cirrus clouds: Three case studies. *J. Atmos. Sci.*, **46,** 371–396.
——, M. Griffin, and G.C. Dodd, 1989b: Optical scattering and microphysical properties of subvisual cirrus clouds, and climatic implications. *J. Appl. Meteor.*, **28,** 91–98.
——, C.J. Grund, J.D. Spinhirne, M.M. Hardesty, and J.M. Alvarez, 1990a: The 27–28 October 1986 FIRE IFO cirrus case study: A five lidar overview of cloud structure and evolution. *Mon. Wea. Rev.*, **118,** 2288–2311.
——, A.W. Huggins, A.B. Long, J.B. Snider, and R.J. Meitin, 1990b: Investigations of a winter mountain storm in Utah. II: Mesoscale structure, supercooled liquid cloud development, and precipitation processes. *J. Atmos. Sci.*, **47,** 1323–1350.
——, H. Zhao, and G.C. Dodd, 1991: Simulated polarization diversity lidar returns from water and precipitating mixed phase clouds. *Appl. Opt.*, **30** (in press).
Schotland, R.M., K. Sassen, and R.J. Stone, 1971: Observations by lidar of linear depolarization ratios by hydrometeors. *J. Appl. Meteor.*, **10,** 1011–1017.
Smiley, V.N., and B.M. Morley, 1981: Lidar depolarization studies of the atmosphere at the South Pole. *Appl. Opt.*, **20,** 2189–2195.
Spinhirne, J.D., and W.D. Hart, 1990: Cirrus structure and radiative parameters from airborne lidar and spectral radiometer observations: 28 October 1986 FIRE case study. *Mon. Wea. Rev.*, **118,** 2329–2343.
——, M.Z. Hansen, and L.O. Caudill, 1982: Cloud top remote sensing by airborne lidar. *Appl. Opt.*, **21,** 1564–1571.
——, ——, and J. Simpson, 1983: The structure and phase of cloud tops as observed by polarization lidar. *J. Climate Appl. Meteor.*, **22,** 1319–1331.
——, R. Boers, and W.D. Hart, 1989: Cloud top liquid water from lidar observations of marine stratocumulus. *J. Appl. Meteor.*, **28,** 81–90.
Sun, Y.-Y., and Z.-P. Li, 1989: Depolarization of polarized light caused by high altitude clouds. Part 2: Depolarization of lidar induced by water clouds. *Appl. Opt.*, **28,** 3633–3638.
——, ——, and J. Bösenberg, 1989: Depolarization of polarized light caused by high altitude clouds. Part 1: Depolarization of lidar induced by cirrus. *Appl. Opt.*, **28,** 3625–3632.
Takano, Y., and K. Jayaweera, 1985: Scattering phase matrix for hexagonal ice crystals computed from ray optics. *Appl. Opt.*, **24,** 3254–3263.
——, and K.-N. Liou, 1989: Solar radiative transfer in cirrus clouds. Part I: Single-scattering and optical properties of hexagonal ice crystals. *J. Atmos. Sci.*, **46,** 3–19.
Takeda, T., and M. Horiguchi, 1986: Simultaneous observation of fine structure of layer clouds at upper and middle levels by a laser radar and an 8.6-mm radar. *J. Meteor. Soc. Japan*, **64,** 109–122.